Depleting Trim28 in adult mice is well tolerated and reduces levels of α-synuclein and tau

Maxime W.C. Rousseaux[1,2], Jean-Pierre Revelli[1,2], Gabriel E. Vázquez-Vélez[2,3,5], Ji-Yoen Kim[1,2], Evelyn Craigen[1,2], Kristyn Gonzales[1,2], Jaclyn Beckinghausen[2,4], Huda Y. Zoghbi[1-4,6,#]

[1] Department of Molecular and Human Genetics, Baylor College of Medicine, Houston, Texas, USA.

[2] Jan and Dan Duncan Neurological Research Institute at Texas Children's Hospital, Houston, Texas, USA.

[3] Program in Developmental Biology, Baylor College of Medicine, Houston, Texas, USA.

[4] Department of Neuroscience, Baylor College of Medicine, Houston, Texas, USA.

[5] Medical Scientist Training Program, Baylor College of Medicine, Houston, TX, USA Howard

[6] Hughes Medical Institute, Baylor College of Medicine, Houston, Texas, USA.

[#]Correspondence: hzoghbi@bcm.edu

Abstract

Alzheimer's and Parkinson's disease are late onset neurodegenerative diseases that will require therapy over decades to mitigate the effects of disease-driving proteins such tau and α-synuclein (α-Syn). We recently found that TRIM28 regulates the levels and toxicity of α-Syn and tau (Rousseaux et al., 2016), however, how TRIM28 regulates α-Syn and whether its chronic inhibition later in life is safe remained unknown. Here, we show that TRIM28 mediates the SUMOylation of α-Syn and tau, and that genetic suppression of Trim28 in adult mice is compatible with life. We were surprised to see that mice lacking Trim28 in adulthood do not exhibit behavioral or pathological phenotypes, and importantly, adult reduction of TRIM28 results in a decrease of α-Syn and tau levels. These results suggest that deleterious effects from TRIM28 depletion are limited to development and that its inhibition adulthood provides a potential path for modulating α-Syn and tau levels.

Introduction

Neurodegenerative disorders such as Alzheimer's disease (AD) and Parkinson's disease (PD) occur in the later decades of life and have no curative therapy. Therefore, future treatments for these disorders must be administered over decades, which means that safety profiles of therapeutic targets are of utmost importance. The advent of alternative therapies such as antisense oligonucleotides, gene therapy and immunotherapy, together with traditional pharmacology have made it such that almost any molecule can be targeted. More and more, the extent to which a target is druggable hitches on the safety and specificity of its targeting over time.

We recently demonstrated that TRIM28 regulates the steady state levels of the neurodegeneration-driving proteins α-Synuclein (α-Syn) and tau (Rousseaux et al., 2016). However, given the critical roles of TRIM28 in mammalian development (Cammas et al., 2000), its tractability as a therapeutic target remains questionable. For instance, complete loss of *Trim28* in mice causes early embryonic lethality due to pre-implantation defects (Cammas et al., 2000), and specific deletion of this gene in the developing tissues cause a host of defects (Cheng et al., 2014; Fasching et al., 2015; Trono, 2015). Moreover, haploinsufficiency of *TRIM28* is expected to have deleterious outcomes in humans (pLI = 1.00, ExAC; (Lek et al., 2016)). This may be due in part due to the multiple functions of TRIM28 within the cell including the repression of endogenous retroviral elements, maintenance of pluripotency, epigenetics and mitophagy (Barde et al., 2013; Czerwinska et al., 2017; Oleksiewicz et al., 2017; Singh et al., 2015; Wolf and Goff, 2009). Given the importance of TRIM28 for development, it remains unclear whether TRIM28 is critical for adult brain function, and whether it may safely be targeted in adulthood. Specifically, two questions remain related to the targeting of TRIM28 pharmacologically: 1) Is there a pharmacologically tractable domain in TRIM28 that could be targeted by a drug? 2) Is genetic

suppression of TRIM28 in the brain and throughout the body tolerated in adulthood? To test this, we performed studies to pinpoint the mechanism by which TRIM28 regulates α-Syn and tau and generated two animal models to disrupt Trim28 in vivo, thus establishing its druggability in adulthood.

Results and Discussion

We previously found that TRIM28 regulates the post-translational stability of α-Syn and tau and that this effect is mediated by two critical cysteines in its RING domain (C65 and C68; (Rousseaux et al., 2016)). We therefore hypothesized that TRIM28 exerted E3 SUMO ligase activity on of α-Syn and tau (Liang et al., 2011; Neo et al., 2015; Yang et al., 2013). To first test whether SUMOylation itself regulates the levels of α-Syn and tau, we inhibited the sole E2 SUMO ligase, UBC9, via RNAi and pharmacological inhibition (using Viomellein (Hirohama et al., 2013)). We found that both approaches were sufficient to decrease α-Syn and tau, suggesting that SUMOylation indeed regulates their steady state levels (**Figure 1A**). We next asked whether TRIM28 mediates the SUMOylation of α-Syn and tau. We first tested this in cells and found that knockdown of endogenous TRIM28 decreased native α-Syn and tau SUMOylation whereas ectopic overexpression of TRIM28 increased their SUMOylation (**Figure 1B**). Interestingly, when we mutated a catalytic RING domain of TRIM28 (C65A/C68A), we could inhibit α-Syn and tau SUMOylation (**Figure 1B**). This was consistent with our previous findings that mutating this residue impeded α-Syn and tau stabilization and nuclear localization (Rousseaux et al., 2016). To next test whether Trim28 regulates α-Syn and tau SUMOylation in vivo, we performed SUMOylation assays on endogenous α-Syn and tau from brain lysates (under

74 denaturing conditions) from wild-type and *Trim28*$^{+/-}$ mice. We found that α-Syn and tau
75 SUMOylation were significantly reduced in *Trim28* haploinsufficient mice (**Figure 1C**).
76 TRIM28 has several important functions throughout the cell, and its loss of function in
77 mice is embryonic lethal. We therefore asked whether one of its domains can be specifically
78 targeted for future therapeutic use without disrupting the others. Given that two conserved
79 critical cysteine residues in its RING domain (**Figure 1-figure supplement 1A**) regulate the
80 bulk of TRIM28 function toward α-Syn and tau, we hypothesized that mutating its endogenous
81 catalytic activity would be the most promising approach. We therefore generated a knockin
82 mouse carrying mutations in its RING domain (**Figure 1-figure supplement 1B**). We found that
83 mutating these residues, despite decreasing α-Syn and tau levels significantly, caused a dramatic
84 destabilization of TRIM28 protein (**Figure 1-figure supplement 1C-D**). Moreover,
85 homozygosing these E3 mutant mice caused embryonic lethality, a feature consistent with the
86 generation of a null allele. Thus, mutating the RING domain of TRIM28 decreases α-Syn and
87 tau levels, but does so by disrupting its structure and stability (**Figure 1-figure supplement 1D**).
88 Since TRIM28 has critical roles in development, we next asked whether we could bypass
89 these defects by knocking down Trim28 in the postnatal mouse brain (**Figure 2-figure**
90 **supplement 1A**). We used an AAV carrying both an shRNA targeting *Trim28* and a YFP
91 reporter. We found that the virus was widely expressed throughout the brain (Kim et al., 2013)
92 and that mice receiving and shRNA against *Trim28* had a 75% depletion of *Trim28* in their brain
93 (**Figure 2-figure supplement 1B**). Importantly, these mice developed normally until at least 10
94 weeks of age. We evaluated cortical and hippocampal thickness and astrocytosis in these mice
95 and did not note any significant defects (**Figure 2-figure supplement 1C**).

Given that synucleinopathies and tauopathies most often occur in the later decades of life, therapeutics should therefore accurately mimic this late-stage disruption. To test whether late stage inhibition of Trim28 is therapeutically tractable, we generated Trim28 adult knockout mice. This was done by crossing a whole body, tamoxifen-inducible Cre (*UBC-CreER^{T2}*, (Ruzankina et al., 2007)) with floxed *Trim28* mice (Cammas et al., 2000). We waited until the animals were 8-12 weeks old before starting a 4-week tamoxifen regimen to ablate *Trim28* (**Figure 2A**). To our surprise, we found that adult depletion did not result in early lethality nor overt phenotypes. Instead, adult knockout mice lived for the duration of the study (30 weeks post tamoxifen injection, **Figure 2B**). We tested whether Trim28 is effectively ablated in these mice and found that Trim28 levels were reduced by over 75% in each tissue tested (both at the RNA and protein level; **Figure 2C, D** and **Figure 2-figure supplement 2A-C**). Importantly, α-Syn and tau levels were also decreased in multiple brain regions, corroborating our previous findings using germline haploinsufficient mice (Rousseaux et al., 2016).

An important aspect of measurable safety margins in the depletion of a gene is its impact on neuronal function. To assess whether loss of Trim28 in adult mice impacts brain structure and function, we performed a battery of behavioral and histological tests. We found that Trim28 adult knockout mice behaved similarly to their control littermate counterparts in every test assayed. Specifically, no defects were observed in motor behavior, anxiety, perseverative movements and memory (**Figure 3A-H**). Consistent with this, we could not discern any gross histological defects nor signs of inflammation (as measured by GFAP immunoreactivity) in the brain (**Figure 4A-C**). We further tested Trim28 levels via immunostaining and found that, while Trim28 was highly expressed in the brain (confirming our western and qPCR results), it was over 75% depleted in the adult knockout (**Figure 4-figure supplement 1A**). A previous study

119 highlighted several gene expression changes in mice lacking Trim28 in forebrain excitatory
120 neurons starting from postnatal day 14 (Jakobsson et al., 2008). We tested the expression of these
121 genes in the hippocampus via qPCR and found that, while the directionality of changes was
122 consistent with the previous study, there was a broad dampening of this effect in the adult
123 knockout mice (**Figure 4-figure supplement 1B**). This may be due to the later stage depletion of
124 Trim28 or the incomplete deletion of Trim28 (there is 15-20% remaining in the adult knockout)
125 and may account for the slight behavioral abnormalities observed in the reported juvenile
126 forebrain-specific Trim28 knockouts (Jakobsson et al., 2008) versus the whole-body adult
127 Trim28 knockouts.

128 Given that the adult knockout affects the whole body, we examined regions of the body
129 that could be vulnerable to Trim28 loss-of-function induced toxicity. We assessed general
130 morphology of the heart, liver and spleen and found no discernable defects in the adult knockout
131 mice compared to littermate controls (**Figure 4-figure supplement 2)**. Moreover, blood
132 chemistry in these mice appeared normal (**Figure 4-figure supplement 3**).

133 Taken together, our study suggests that adult depletion of more than 75% of total Trim28
134 from the mouse body is safe. This is consistent with reports that deletion of TRIM28 in
135 terminally differentiated muscle is safe (Dalgaard et al., 2016). These findings hold important
136 implications for therapeutic targeting of Trim28 in diseases such as AD and PD where an
137 inhibitor targeting TRIM28 may hold promise in the future. An important point of consideration
138 moving forward into therapeutics is the mechanism by which TRIM28 regulates the steady state
139 levels of α-Syn and tau. While our data suggest that TRIM28 forms a complex with α-Syn and
140 tau (Rousseaux et al., 2016) and mediates their SUMOylation, we were not able to reconstitute
141 this complex in a cell-free system, suggesting that other factors may be at play. Furthermore,

while disruption of TRIM28 E3 ligase activity in vivo reduced α-Syn and tau levels, it likely did so by destabilization of TRIM28 itself. Thus, it is still unclear whether this inhibition represents a loss of enzymatic function or simply a structural loss. Further studies looking at the effect of this inhibition in adulthood or targeting other domains that may mediate TRIM28 SUMOylation may hold promise. For instance, the bromodomain of TRIM28 could be an alternative target given that a mutation in cysteine 651 to an alanine (C651A) reduces its SUMOylation activity on another target, VPS34 (Yang et al., 2013). Most importantly, this study highlights the importance of testing the loss of function of lethal variants in the adult. While databases such as ExAC and GnomAD (Lek et al., 2016) offer a window into the pathogenicity of variants in development, it should not be the only factor guiding target selection; especially for neurodegenerative conditions where treatment will often only occur in the later decades of life.

Materials and methods

SUMOylation assays

α-Syn and tau SUMOylation were assayed in cells as follows. Briefly, HEK293T cells were transfected with 3 µg Flag-SUMO2 and TRIM28 variants for 48 hours. Cells were harvested in cold PBS and spun down at 5,000 RPM for five minutes at 4°C. Cells were then lysed in SUMO lysis buffer (1 % Triton X-100, 150 mM NaCl, 10 mM Tris pH 8.0, 10 % glycerol, 20 mM N-ethyl maleimide and protease inhibitors [Roche]) for 40 minutes on ice with occasional vortexing. Cell debris were spun down at 15,000 RPM for 20 minutes at 4°C. Lysates were applied to Dynabeads (Protein G, 15µL slurry) that were previously washed and then conjugated to 1 µg of antibody (α-Syn, C-20 Santa Cruz Biotechnology; tau, tau-5 Abcam) and incubated with rotation for 2 hours at 4°C. This sub-threshold pull-down allowed us to bypass the regulatory effect of TRIM28 on α-Syn and tau. Bound proteins were vigorously washed (to remove any interactors which themselves may be SUMOylated) four times in 500 µL of SUMO lysis buffer and eluted for 10 minutes at 95°C for downstream western blot analysis. For each condition, either cell lines stably knocking down *TRIM28* (*shTRIM28*) or non-silencing (*shScramble*) were used. In addition, TRIM28, TRIM28-Mut and control constructs were co-transfected at 300 ng per well (1:10 ratio to SUMO concentration). Alternatively, Flag-SUMO2 was pulled down using Flag-M2 magnetic beads (20 µl slurry, Sigma) under denaturing conditions (first boiling the sample prior to the IP). Each SUMOylation assay was performed three independent times.

For the *in vivo* SUMOylation assay, mouse brains were harvested in RIPA buffer containing protease and phosphatase inhibitors (GenDepot). Samples were boiled for 5 minutes at 95ºC, following which antibodies (2.5 µg) targeting α-Syn (C-20, SCBT) or Tau (Tau-5,

Abcam) were incubated overnight with rotation at 4ºC. Antibody-lysate complexes were bound to Dynabeads (25 µl, Protein G) for 2 hours at 4ºC with rotation and then washed vigorously 5 x 1 mL in wash buffer (50 mM Tris pH 7.3, 170 mM NaCl, 1 mM EDTA, 0.5 % NP-40). Bound protein was eluted in Laemlli buffer at 85ºC for 10 minutes. Lysates were run on SDS-PAGE followed by Western blot and SUMOylated species were detected by probing for SUMO2/3 (Abcam).

Generation of Trim28^{E3MT} *mice.*

Trim28^{E3MT} mice were generated via CRISPR/Cas9-mediated gene editing (Wang et al., 2013). Briefly, an sgRNA targeting the 5' of *Trim28* was synthesized by direct PCR from pX330 (gift from Zhang lab, Addgene #42230) and *in vitro* transcribed with the MEGAshortscript T7 Transcription kit (Invitrogen) using the following two primers (forward: 5'-TTAATACGACTCACTATAGGGCGTGTGTCGCGAGCGCCTGGTTTTAGAGCTAGAAAT AGC-3'; reverse: 5'-AAAAGCACCGACTCGGTGCC-3'). A single stranded oligodeoxynucleotide (ssODN) was purchased from IDT for homologous-directed recombination introducing the C66A, C69A and R72G mutations in Trim28 (5'-CTGCAGCCGCGTCGTCCCCTGCGGGGGGCGGTGGCGAGGCGCAGGAGCTTTTAGAA CATGCCGGTGTCGCCAGGGAAGGACTCAGACCAGAACGGGATCCTCGGCTGCTGCC CTGTCTACATTCGGCCTGCAGTGCCTGCCTGGGCCCCGCTACACCCGCCGCAGCGAA TAATTCGGGGGATGGCGGCTCGG-3'). The PAM (protospacer adjacent motif) and additional adjacent synonymous mutations were introduced to increase editing efficiency and allow for simple genotyping by differential primer hybridization. On the day of injection, Cas9 protein (PNA Bio), sgRNA and repair template (ssODN) were injected (pronuclear) into ova from C57Bl/6 female mice and transferred into oviducts of pseudopregnant females. The

following primers were used to distinguish the E3 mutant allele (forward: 5'-TTGGCGGCGAGCGCACTTGC-3'; reverse: 5'-CCCTGGCGACACCGGCATG-3' or forward: 5'-CATGCCGGTGTCGCCAGGGA-3'; reverse: 5'-TCCCACAGGACATACCTGGTTAGCATCCTGG-3') from the wildtype allele (forward: 5'-TTGGCGGCGAGCGCACTTGC-3'; reverse: 5'-TCGCGACACACGCCGCAGTG-3' or 5'-CACTGCGGCGTGTGTCGCGA-3'; reverse: 5'-TCCCACAGGACATACCTGGTTAGCATCCTGG-3'). Founder mice were backcrossed at least three times prior to experimentation to get rid of potential off-target mutations.

Tamoxifen injections

Tamoxifen injections were performed as previously described (Sztainberg et al., 2015). Briefly, starting at 8-12 weeks of age, tamoxifen or vehicle (peanut oil) was injected intraperitoneally at a dose of 100 mg/kg, three times a week for four weeks. Mice were left to recover for at least two weeks before proceeding with behavioral, biochemical and histological assessment.

AAV generation and P0 injections

An AAV8 vector containing both YFP and a miRE cassette-containing shRNA (Fellmann et al., 2013) under the control of the chicken beta actin (CBA) promoter was generated using Gibson cloning. Individual shRNA sequences were generating using the splaSH algorithm (Pelossof et al., 2017). Each shRNA vector was tested for efficiency in Neuro2A cells prior to virus generation. Briefly, Neuro2A cells ($1x10^5$) were plated in 24-well plates and transfected with 500 ng of each vector using Lipofectamine 3000 (ThermoFisher Scientific, L3000150). Transfection efficiency was measured by looking at YFP fluorescence (average ~60-75% cells infected) and knockdown efficiency was determined by qPCR. AAV production and titering was performed as previously described (Kim et al., 2008).

AAV delivery was carried out in neonatal (P0) FVB mouse pups as previously described (Kim et al., 2013). Briefly, neonatal pups (<8 hours from birth) were separated from lactating dams and anesthetized on ice. $1x10^{11}$ viral genomes were injected per ventricle (total of $2x10^{11}$ genomes per mouse) and mice were left to recover on a heated pad before returning them to their mother. All procedures were performed in a BSL2-contained area and mouse bedding and housing was changed 72 hours post injection. Virus expression confirmation was performed using a BlueStar UV light (Electron Microscopy Sciences) at three days post injection. Tissue from the caudal region of the cerebrum (cortex + hippocampus) was harvested ten weeks post injection as this region had the maximal viral expression (YFP positive signal) and offered optimal *Trim28* knockdown by qPCR. Flash frozen tissue was homogenized in a 1.5mL eppendorf containing 10 µl/mg of PEPI buffer (1x PBS containing 5 mM EDTA, protease inhibitor cocktail and RNAse inhibitor cocktail) using an electric pestle. The resulting homogenate was split in a 3:1 ratio for downstream protein (3 parts) and RNA (1 part) applications. RNA extraction was performed using the RNeasy mini kit (Qiagen) whereas protein extraction was performed by adding equal volumes of 2x RIPA buffer (100 mM Tris pH 8.0, 300 mM NaCl, 0.2% Sodium dodecyl sulfate [SDS], 1% Sodium Deoxycholate, 2% Nonidet P-40, 5 mM EDTA, protease and phosphatase inhibitor cocktails) vortexing and incubating samples on ice for 20 minutes before spinning lysates down at 16,000g for 20 minutes at 4°C.

Behavioral analysis

Behavioral analysis was performed by an experimenter blind to the treatment and genotype of the animals. Animal behavior was conducted between 10 am and 4 pm for each test and was carried out when the animals were 14-22 weeks old (6-10 weeks post tamoxifen injection). The open-field analysis (Lu et al., 2017), parallel rod footslip (Ure et al., 2016), pole test (Rousseaux

et al., 2012), elevated plus maze (Lu et al., 2017), conditioned fear (Lu et al., 2017), novel object recognition (Antunes and Biala, 2012), hole poke (Ito-Ishida et al., 2015) and rotarod (Lasagna-Reeves et al., 2015) were performed as previously described. For each test, mice were left to habituate in the testing room with ambient white noise for 30-60 minutes prior to testing.

Histological analysis

For frozen sections: Free floating sections (25 µm) were mounted and dried on polarized slides (>48h). Slides were then stained for Cresyl violet and GFAP as previously described (Rousseaux et al., 2016). For GFAP quantification, photomicrographs were taken using the 10x objective on a Leica DM4000 LED. The percentage of immunoreactive area for GFAP was calculated using ImageJ. Briefly, each DAB-stained image was converted to 8-bit greyscale and made into a binary image using a threshold cutoff of 10% for a representative WT section (after which, the same settings were used for all of the sections in question). Area of interest (Hippocampus or Cortex) was outlined and total area was measured. Within this area, the "Analyze particles" function was used to determine the area of each outlined immunoreactive entity. The sum of these entities was set at the GFAP positive area and the percentage immunoreactive area was presented as GFAP positive area compared to total area (in %). For cresyl violet staining, the relative width of either the caudal cortex or the CA1 region of the hippocampus was measured in four independent sections.

For paraffin-embedded sections: Formalin-fixed tissues were embedded in paraffin and sectioned on a microtome at 5 µm thickness. Sections were deparaffinized in a series of xylene and ethanol washes before being subjected to antigen retrieval for 10 minutes at 95^{o}C in a buffer containing 10 mM sodium citrate and 0.02% Tween (pH 6.0). Sections were then blocked for one hour at room temperature in PBS + 0.3% Triton X-100 and 5% FBS and stained in blocking

buffer containing either 1:400 anti-GFAP (GA5, Sigma) or 1:500 anti-Trim28 (20C1, Abcam) and corresponding secondary antibodies (Vectastain mouse elite ABC kit or Donkey anti-mouse Alexa 488 secondary). Fluorescent sections were counterstained using DAPI. Gross morphology was assessed by performing hematoxylin and eosin (H&E) staining using standard protocols.

Mouse blood collection

Mice were anaesthetized with isoflurane and blood was collected from the retro-orbital sinus. The animal under general anesthesia is gently scruffed and a capillary is inserted into the medial canthus of the eye. Applying a slight pressure to the capillary allows the blood flow to be directed to a collection tube. After letting the blood coagulate for 30 min, the serum is collected post centrifugation 4 minutes at 14,000 rpm for analyte analysis with Charles River Laboratories.

Acknowledgements

The authors thank members of the Zoghbi lab for important discussions and critical feedback on the manuscript, L.A. Lavery for helping with TRIM28 structural modeling experiments and A. Hatcher and J. Noebels for the *Mapt*$^{-/-}$ mice. This research was supported in part by the Robert A. and Renée E. Belfer Family Foundation, the Huffington Foundation, The Hamill Foundation, the Howard Hughes Medical Institute and UCB Pharma (H.Y.Z.), the Parkinson's Foundation Stanley Fahn Junior Faculty Award PF-JFA-1762 (M.W.C.R.), the behavior, pathology, RNA in situ hybridization and confocal cores at the Jan and Dan Duncan Neurological Research Institute and the BCM Intellectual and Developmental Disabilities Research Center (NIH U54 HD083092 from the Eunice Kennedy Shriver National Institute of Child Health & Human Development). The IDDRC Microscopy Core was used for this project. The content is solely the responsibility

of the authors and does not necessarily represent the official views of the Eunice Kennedy Shriver National Institute of Child Health and Human Development or the National Institutes of Health.

Competing interests: The authors have no competing interests to declare.

References:

Antunes, M., and Biala, G. (2012). The novel object recognition memory: neurobiology, test procedure, and its modifications. Cogn Process *13*, 93-110.

Barde, I., Rauwel, B., Marin-Florez, R.M., Corsinotti, A., Laurenti, E., Verp, S., Offner, S., Marquis, J., Kapopoulou, A., Vanicek, J.*, et al.* (2013). A KRAB/KAP1-miRNA cascade regulates erythropoiesis through stage-specific control of mitophagy. Science *340*, 350-353.

Cammas, F., Mark, M., Dolle, P., Dierich, A., Chambon, P., and Losson, R. (2000). Mice lacking the transcriptional corepressor TIF1beta are defective in early postimplantation development. Development *127*, 2955-2963.

Cheng, C.T., Kuo, C.Y., and Ann, D.K. (2014). KAPtain in charge of multiple missions: Emerging roles of KAP1. World journal of biological chemistry *5*, 308-320.

Czerwinska, P., Shah, P.K., Tomczak, K., Klimczak, M., Mazurek, S., Sozanska, B., Biecek, P., Korski, K., Filas, V., Mackiewicz, A.*, et al.* (2017). TRIM28 multi-domain protein regulates cancer stem cell population in breast tumor development. Oncotarget *8*, 863-882.

Dalgaard, K., Landgraf, K., Heyne, S., Lempradl, A., Longinotto, J., Gossens, K., Ruf, M., Orthofer, M., Strogantsev, R., Selvaraj, M.*, et al.* (2016). Trim28 Haploinsufficiency Triggers Bi-stable Epigenetic Obesity. Cell *164*, 353-364.

Fasching, L., Kapopoulou, A., Sachdeva, R., Petri, R., Jonsson, M.E., Manne, C., Turelli, P., Jern, P., Cammas, F., Trono, D.*, et al.* (2015). TRIM28 represses transcription of endogenous retroviruses in neural progenitor cells. Cell Rep *10*, 20-28.

Fellmann, C., Hoffmann, T., Sridhar, V., Hopfgartner, B., Muhar, M., Roth, M., Lai, D.Y., Barbosa, I.A., Kwon, J.S., Guan, Y.*, et al.* (2013). An optimized microRNA backbone for effective single-copy RNAi. Cell Rep *5*, 1704-1713.

322 Hirohama, M., Kumar, A., Fukuda, I., Matsuoka, S., Igarashi, Y., Saitoh, H., Takagi, M., Shin-
323 ya, K., Honda, K., Kondoh, Y., *et al.* (2013). Spectomycin B1 as a novel SUMOylation inhibitor
324 that directly binds to SUMO E2. ACS Chem Biol *8*, 2635-2642.
325 Ito-Ishida, A., Ure, K., Chen, H., Swann, J.W., and Zoghbi, H.Y. (2015). Loss of MeCP2 in
326 Parvalbumin-and Somatostatin-Expressing Neurons in Mice Leads to Distinct Rett Syndrome-
327 like Phenotypes. Neuron *88*, 651-658.
328 Jakobsson, J., Cordero, M.I., Bisaz, R., Groner, A.C., Busskamp, V., Bensadoun, J.C., Cammas,
329 F., Losson, R., Mansuy, I.M., Sandi, C., *et al.* (2008). KAP1-mediated epigenetic repression in
330 the forebrain modulates behavioral vulnerability to stress. Neuron *60*, 818-831.
331 Kim, J., Miller, V.M., Levites, Y., West, K.J., Zwizinski, C.W., Moore, B.D., Troendle, F.J.,
332 Bann, M., Verbeeck, C., Price, R.W., *et al.* (2008). BRI2 (ITM2b) inhibits Abeta deposition in
333 vivo. J Neurosci *28*, 6030-6036.
334 Kim, J.Y., Ash, R.T., Ceballos-Diaz, C., Levites, Y., Golde, T.E., Smirnakis, S.M., and
335 Jankowsky, J.L. (2013). Viral transduction of the neonatal brain delivers controllable genetic
336 mosaicism for visualising and manipulating neuronal circuits in vivo. Eur J Neurosci *37*, 1203-
337 1220.
338 Lasagna-Reeves, C.A., Rousseaux, M.W., Guerrero-Munoz, M.J., Vilanova-Velez, L., Park, J.,
339 See, L., Jafar-Nejad, P., Richman, R., Orr, H.T., Kayed, R., *et al.* (2015). Ataxin-1 oligomers
340 induce local spread of pathology and decreasing them by passive immunization slows
341 Spinocerebellar ataxia type 1 phenotypes. Elife *4*.
342 Lek, M., Karczewski, K.J., Minikel, E.V., Samocha, K.E., Banks, E., Fennell, T., O'Donnell-
343 Luria, A.H., Ware, J.S., Hill, A.J., Cummings, B.B., *et al.* (2016). Analysis of protein-coding
344 genetic variation in 60,706 humans. Nature *536*, 285-291.

345 Liang, Q., Deng, H., Li, X., Wu, X., Tang, Q., Chang, T.H., Peng, H., Rauscher, F.J., 3rd, Ozato,
346 K., and Zhu, F. (2011). Tripartite motif-containing protein 28 is a small ubiquitin-related
347 modifier E3 ligase and negative regulator of IFN regulatory factor 7. J Immunol *187*, 4754-4763.
348 Lu, H.C., Tan, Q., Rousseaux, M.W., Wang, W., Kim, J.Y., Richman, R., Wan, Y.W., Yeh, S.Y.,
349 Patel, J.M., Liu, X.*, et al.* (2017). Disruption of the ATXN1-CIC complex causes a spectrum of
350 neurobehavioral phenotypes in mice and humans. Nat Genet *49*, 527-536.
351 Neo, S.H., Itahana, Y., Alagu, J., Kitagawa, M., Guo, A.K., Lee, S.H., Tang, K., and Itahana, K.
352 (2015). TRIM28 Is an E3 Ligase for ARF-Mediated NPM1/B23 SUMOylation That Represses
353 Centrosome Amplification. Mol Cell Biol *35*, 2851-2863.
354 Oleksiewicz, U., Gladych, M., Raman, A.T., Heyn, H., Mereu, E., Chlebanowska, P.,
355 Andrzejewska, A., Sozanska, B., Samant, N., Fak, K.*, et al.* (2017). TRIM28 and Interacting
356 KRAB-ZNFs Control Self-Renewal of Human Pluripotent Stem Cells through Epigenetic
357 Repression of Pro-differentiation Genes. Stem Cell Reports *9*, 2065-2080.
358 Pelossof, R., Fairchild, L., Huang, C.H., Widmer, C., Sreedharan, V.T., Sinha, N., Lai, D.Y.,
359 Guan, Y., Premsrirut, P.K., Tschaharganeh, D.F.*, et al.* (2017). Prediction of potent shRNAs with
360 a sequential classification algorithm. Nat Biotechnol *35*, 350-353.
361 Rousseaux, M.W., de Haro, M., Lasagna-Reeves, C.A., De Maio, A., Park, J., Jafar-Nejad, P.,
362 Al-Ramahi, I., Sharma, A., See, L., Lu, N.*, et al.* (2016). TRIM28 regulates the nuclear
363 accumulation and toxicity of both alpha-synuclein and tau. Elife *5*.
364 Rousseaux, M.W., Marcogliese, P.C., Qu, D., Hewitt, S.J., Seang, S., Kim, R.H., Slack, R.S.,
365 Schlossmacher, M.G., Lagace, D.C., Mak, T.W.*, et al.* (2012). Progressive dopaminergic cell
366 loss with unilateral-to-bilateral progression in a genetic model of Parkinson disease. Proc Natl
367 Acad Sci U S A *109*, 15918-15923.

368 Ruzankina, Y., Pinzon-Guzman, C., Asare, A., Ong, T., Pontano, L., Cotsarelis, G., Zediak, V.P.,
369 Velez, M., Bhandoola, A., and Brown, E.J. (2007). Deletion of the developmentally essential
370 gene ATR in adult mice leads to age-related phenotypes and stem cell loss. Cell Stem Cell *1*,
371 113-126.
372 Singh, K., Cassano, M., Planet, E., Sebastian, S., Jang, S.M., Sohi, G., Faralli, H., Choi, J.,
373 Youn, H.D., Dilworth, F.J.*, et al.* (2015). A KAP1 phosphorylation switch controls MyoD
374 function during skeletal muscle differentiation. Genes Dev *29*, 513-525.
375 Trono, D. (2015). Transposable Elements, Polydactyl Proteins, and the Genesis of Human-
376 Specific Transcription Networks. Cold Spring Harb Symp Quant Biol *80*, 281-288.
377 Ure, K., Lu, H., Wang, W., Ito-Ishida, A., Wu, Z., He, L.J., Sztainberg, Y., Chen, W., Tang, J.,
378 and Zoghbi, H.Y. (2016). Restoration of Mecp2 expression in GABAergic neurons is sufficient
379 to rescue multiple disease features in a mouse model of Rett syndrome. Elife *5*.
380 Wang, H., Yang, H., Shivalila, C.S., Dawlaty, M.M., Cheng, A.W., Zhang, F., and Jaenisch, R.
381 (2013). One-step generation of mice carrying mutations in multiple genes by CRISPR/Cas-
382 mediated genome engineering. Cell *153*, 910-918.
383 Wolf, D., and Goff, S.P. (2009). Embryonic stem cells use ZFP809 to silence retroviral DNAs.
384 Nature *458*, 1201-1204.
385 Yang, Y., Fiskus, W., Yong, B., Atadja, P., Takahashi, Y., Pandita, T.K., Wang, H.G., and
386 Bhalla, K.N. (2013). Acetylated hsp70 and KAP1-mediated Vps34 SUMOylation is required for
387 autophagosome creation in autophagy. Proc Natl Acad Sci U S A *110*, 6841-6846.

388

389

Author Contributions

M.W.C.R. and H.Y.Z. conceived the study, designed experiments, analyzed and interpreted the data and wrote the manuscript. M.W.C.R., J.-P.R. and J.B. performed molecular and biochemical experiments. M.W.C.R., J.-P.R., G. E. V.-V., J.-Y.K., and E.C. performed mouse genotyping, injections, histology and microscopy.

396 **Figures**

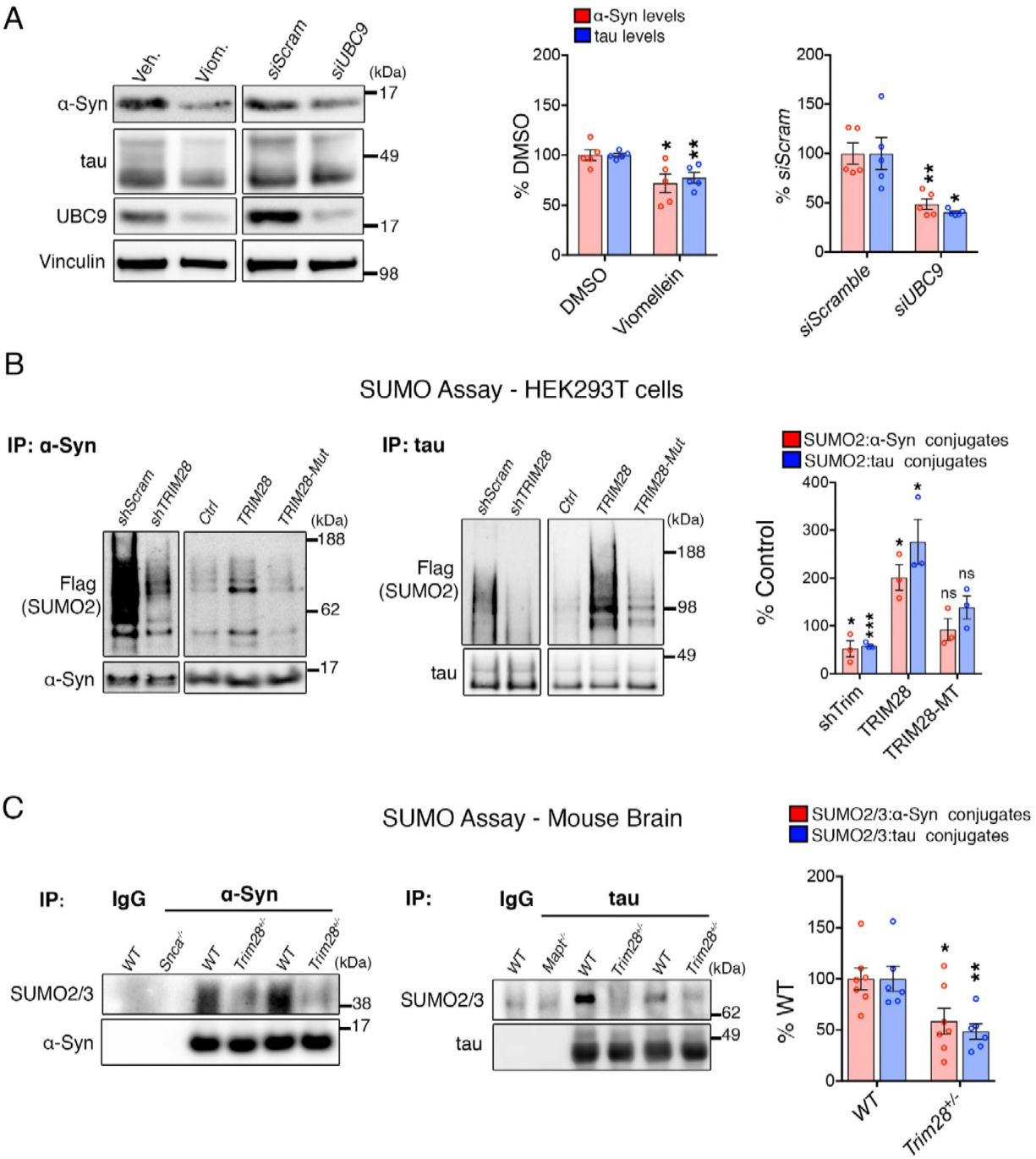

Figure 1

397

Figure 1. Trim28 mediates the SUMOylation of α-Syn and tau. (**A**) Blocking SUMOylation – by either pharmacological inhibition using viomellein or siRNA-mediated suppression of the sole SUMO E2 ligase, UBC9 – decreases α-Syn and tau levels by western blot. (**B**) SUMO assay in human cells reveals that TRIM28 mediates the formation of SUMO2 adducts on α-Syn and tau. This effect is lost upon mutation of the RING domain of TRIM28 (TRIM28-Mut). (**C**) *In vivo* SUMO assay from denatured mouse brain lysates of WT and *Trim28*$^{+/-}$ mice. *Snca*$^{-/-}$ and *Mapt*$^{-/-}$ mice and IP: IgG serve as negative controls. *, **, *** and ns denote $P < 0.05$, $P < 0.01$, $P < 0.001$ and $P > 0.05$, respectively.

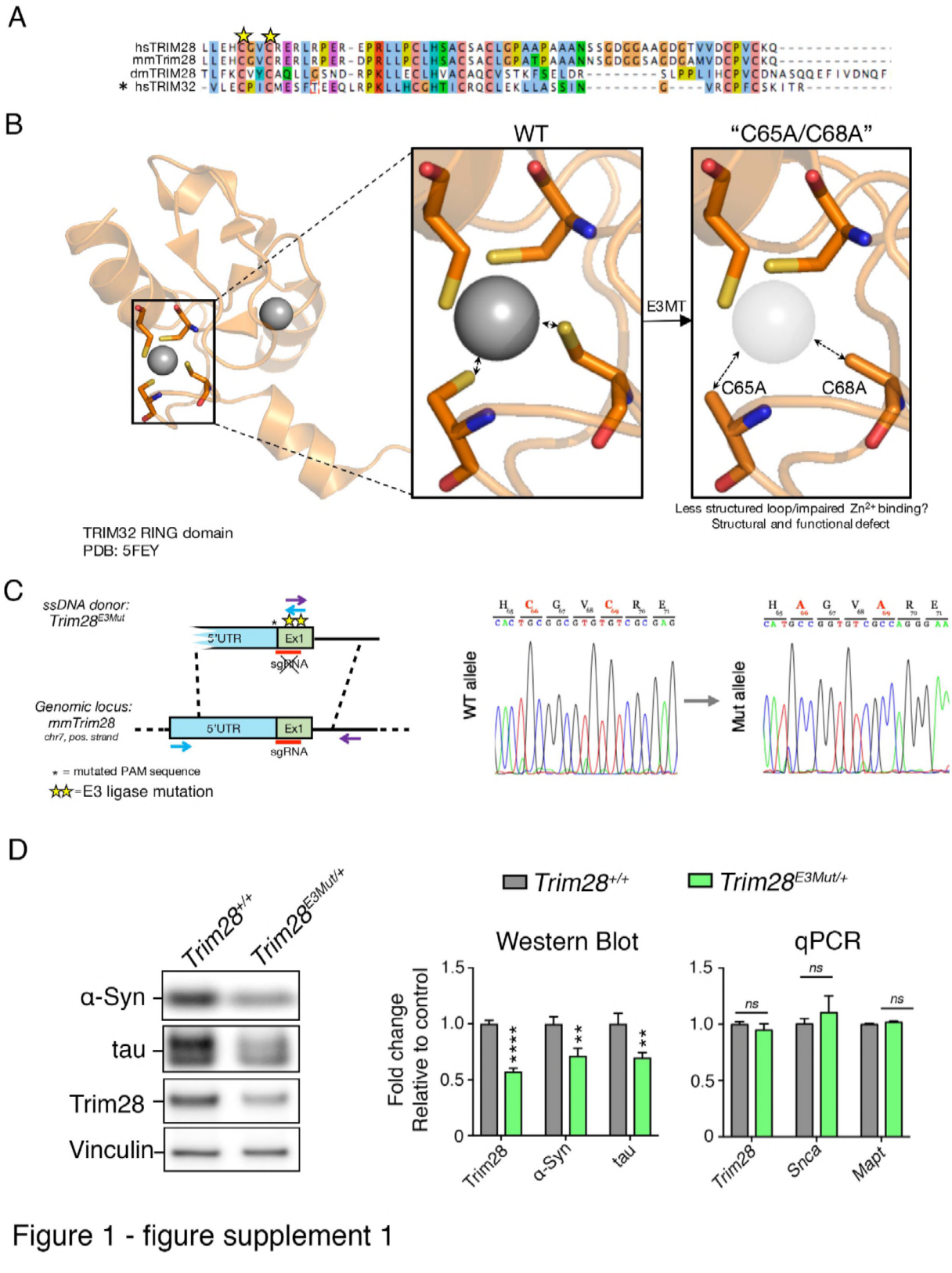

Figure 1 - figure supplement 1

Figure 1-figure supplement 1. Ablating endogenous Trim28 catalytic activity dramatically reduces its

407 stability, concomitantly decreasing α-Syn and tau levels. (**A**), Structural rationale for targeting the RING
408 domain of Trim28. Alignment of human TRIM28 (hsTRIM28) with mouse (mmTrim28) and *Drosophila*
409 *melanogaster* (dmTRIM28) TRIM28 in addition to human TRIM32 (hsTRIM32). * denotes the sequence
410 upon which modeling was conducted. Modeling of RING domain disruption in PyMOL using the
411 TRIM32 RING domain (PDB: 5FEY). (**B**), Approach to mutate endogenous Trim28 catalytic activity
412 and sanger sequencing confirmation of mutation insertion. (**C**), Western blot and qPCR analysis of
413 *Trim28, Snca* and *Mapt* transcripts in Trim28 E3 mutant heterozygous mice ($Trim28^{E3MT/+}$) compared to
414 littermate controls. In (**C**), n = 4-9 mice per genotype. Error bars denote s.e.m. **, **** and ns denote $P <$
415 0.01, $P < 0.0001$ and $P > 0.05$, respectively.

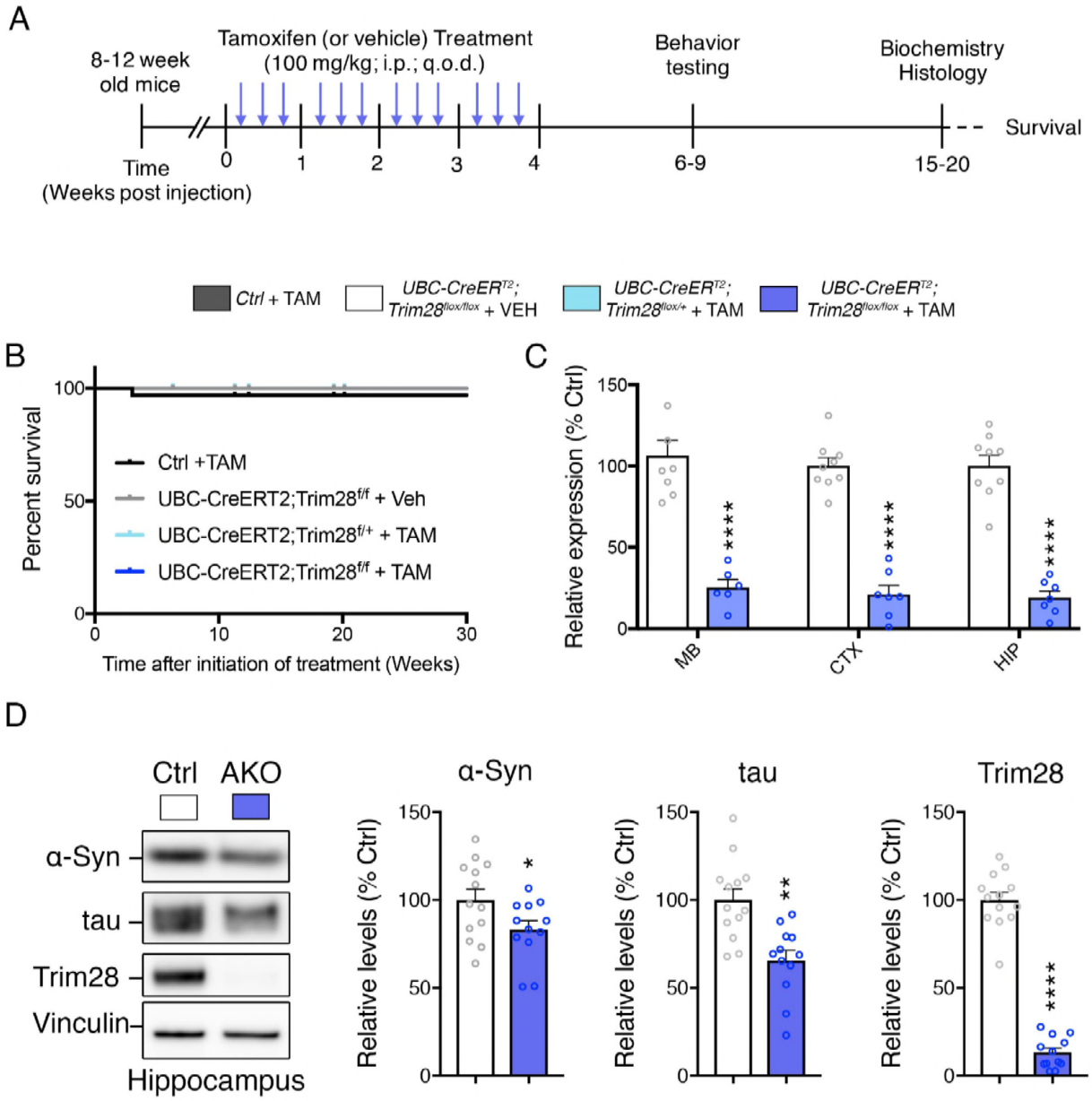

Figure 2

Figure 2. Trim28 adult knockout mice are viable and demonstrate reduced α-Syn and tau levels. (**A**)

418 Experimental approach to delete Trim28 from the adult body. (**B**) Kaplan-Meier survival curve of Adult
419 knockout mice (*UBC-CRE^{ERT2}; Trim28$^{flox/flox}$* + TAM vs littermate controls). No significant differences in
420 survival are observed. (**C**) qPCR analysis for Trim28 expression in midbrain (MB), cortex (CTX) and
421 hippocampus (HIP) of Trim28 adult knockout mice and control littermates. (**D**) Western blot analysis of
422 α-Syn, tau and Trim28 levels in hippocampi from Trim28 adult knockout mice and control littermates. In
423 (**B**), *n* = 14-33 per group. In (**C** and **D**), *n* = 12-13 per group.

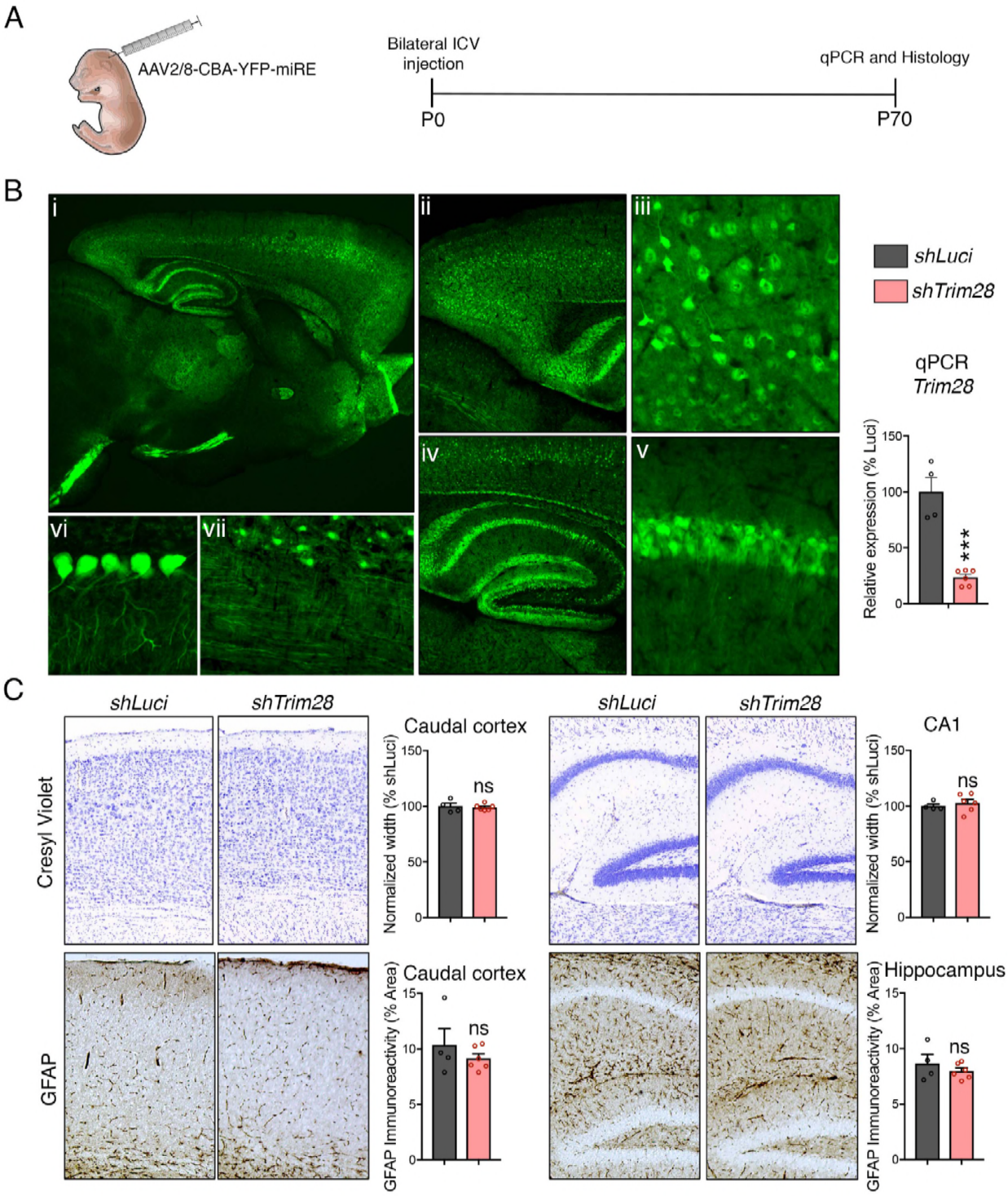

Figure 2 - figure supplement 1

Figure 2-figure supplement 1. Perinatal suppression of Trim28 in the brain is safe and decreases α-Syn

and tau levels. (**A**) Approach to deplete Trim28 in the postnatal brain via RNAi. (**B**) Left panel demonstrates widespread expression of AAV across the brain. Epifluorescence of YFP expression in a representative 10-week-old mouse demonstrating widespread expression of the AAV throughout various brain regions. Brain regions depicted: i) whole forebrain; ii) caudal cortex; iii) caudal cortex (zoom); iv) hippocampus; v) hippocampal CA1 region (zoom); vi) Purkinje cells; and vii) brainstem). Right panel denotes evidence of *Trim28* depletion by qPCR from mice harboring AAV-encoded shRNAs against *Trim28* (*shTrim28*) compared to control, shRNAs against Luciferase (*shLuci*). (**C**) Histological examination at the level of the cortex (left panel) and hippocampus (right panel) of mice expressing *shTrim28* or *shLuci*. Cortical and CA1 thickness are measured via cresyl violet staining and astrogliosis is measured using GFAP staining. In (**B**) and (**C**), $n = 4\text{-}6$. *** and ns denote $P < 0.001$ and $P > 0.05$, respectively.

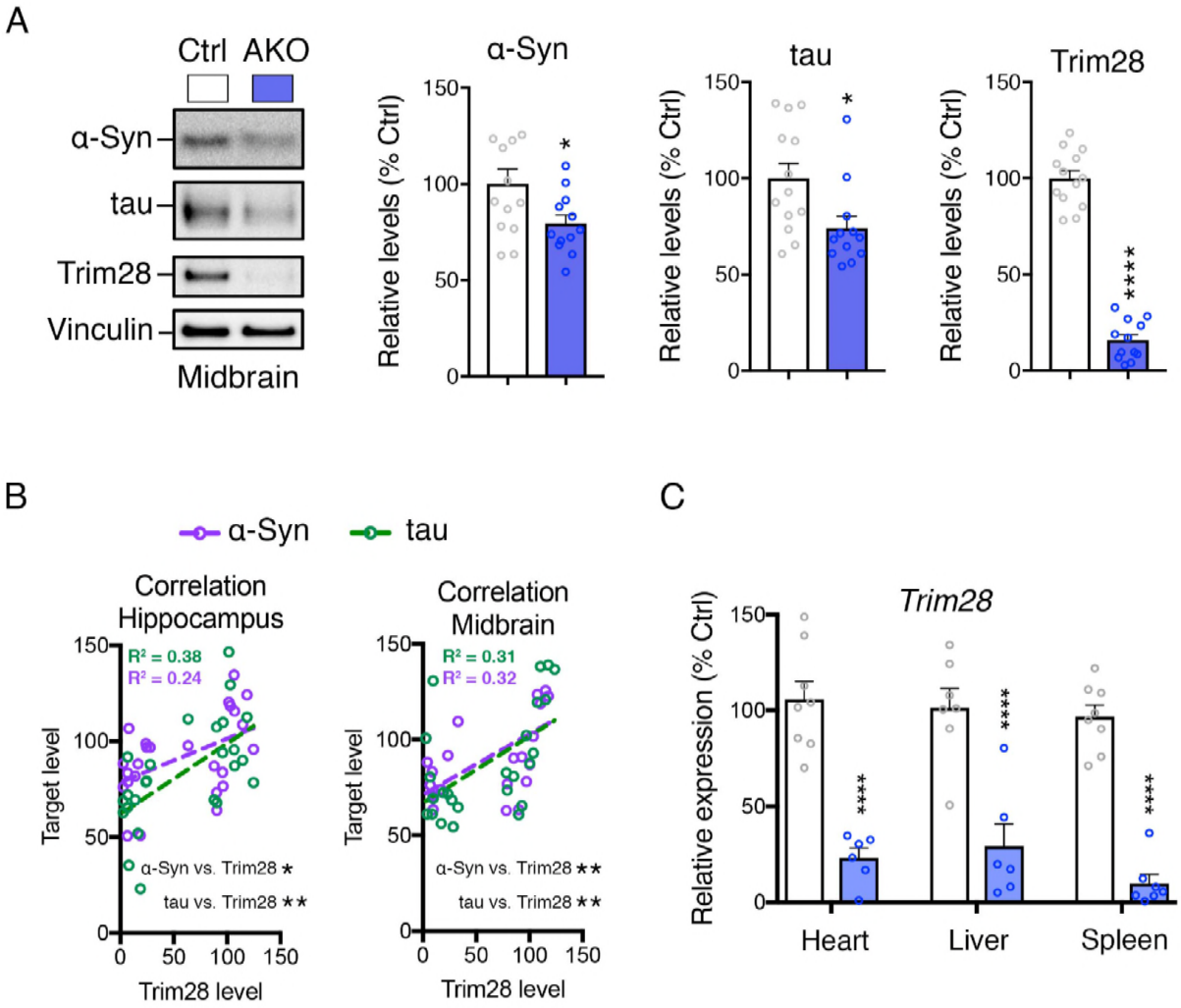

Figure 2 - figure supplement 2

Figure 2-figure supplement 2. α-Syn and tau levels are reduced in multiple brain regions from Trim28

adult knockout mice. (**A**) Western blot analysis of α-Syn, tau and Trim28 levels in the midbrain from adult knockout mice and littermate controls. (**B**) Correlation analysis between Trim28 levels and α-Syn or tau levels in hippocampal or midbrain extracts from Trim28 adult knockout mice and littermate controls. R^2 values are presented for each linear regression. (**C**) qPCR analysis of *Trim28* expression from peripheral organs in adult knockout mice and littermate controls. In (**A** and **B**), n = 12-13 per group. In (**C**), n = 7-8 per group. *, ** and **** denote $P < 0.05$, $P < 0.01$ and $P < 0.001$, respectively.

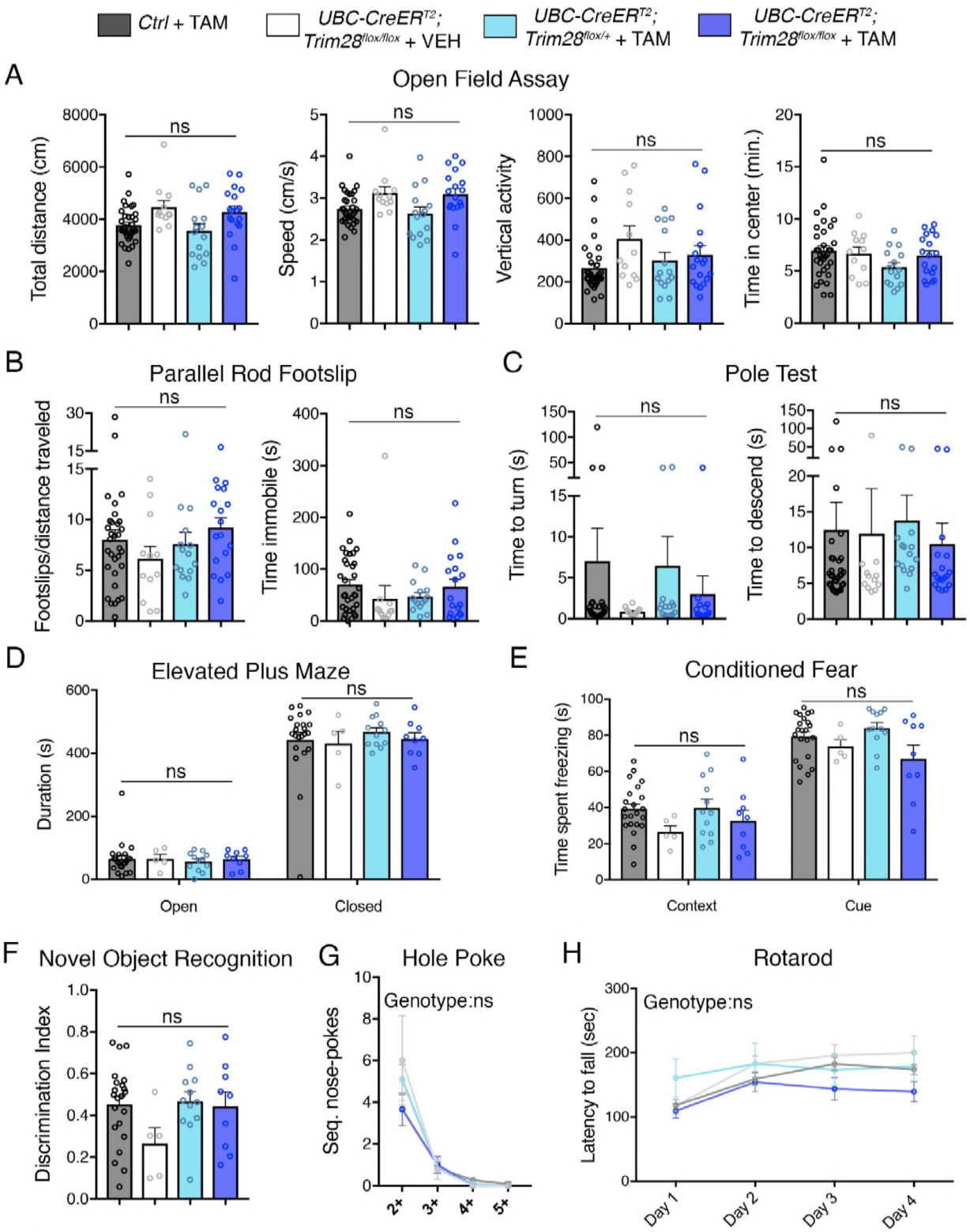

Figure 3

Figure 3. Adult depletion of Trim28 does not cause behavioral abnormalities. Adult knockout mice and

littermate controls were subjected to: (**A**) Open field assay where total distance, speed, vertical activity and time in center were measured over a period of 30 minutes. (**B**) Parallel rod footslip analysis where number of footslips and time spent immobile were measured on a grid over a period of 10 minutes. (**C**) Pole test where the time to turn and descend were measured to a mouse on top (facing upward) of a 18" pole. (**D**) Elevated plus maze measured the time spent in open vs. closed arms during a period of 10 minutes. (**E**) Pavlovian conditioned fear analysis in both context and cued settings (day 2). (**F**) Novel object recognition assay showing the discrimination index for identifying the novel vs. familiar object. (**G**) Hole poke analysis of repetitive behavior measuring the number of sequential nose pokes. (**H**) Rotarod analysis measuring the motor coordination and learning of mice over a period of four days. For each test, n = 5-33; ns denotes $P > 0.05$.

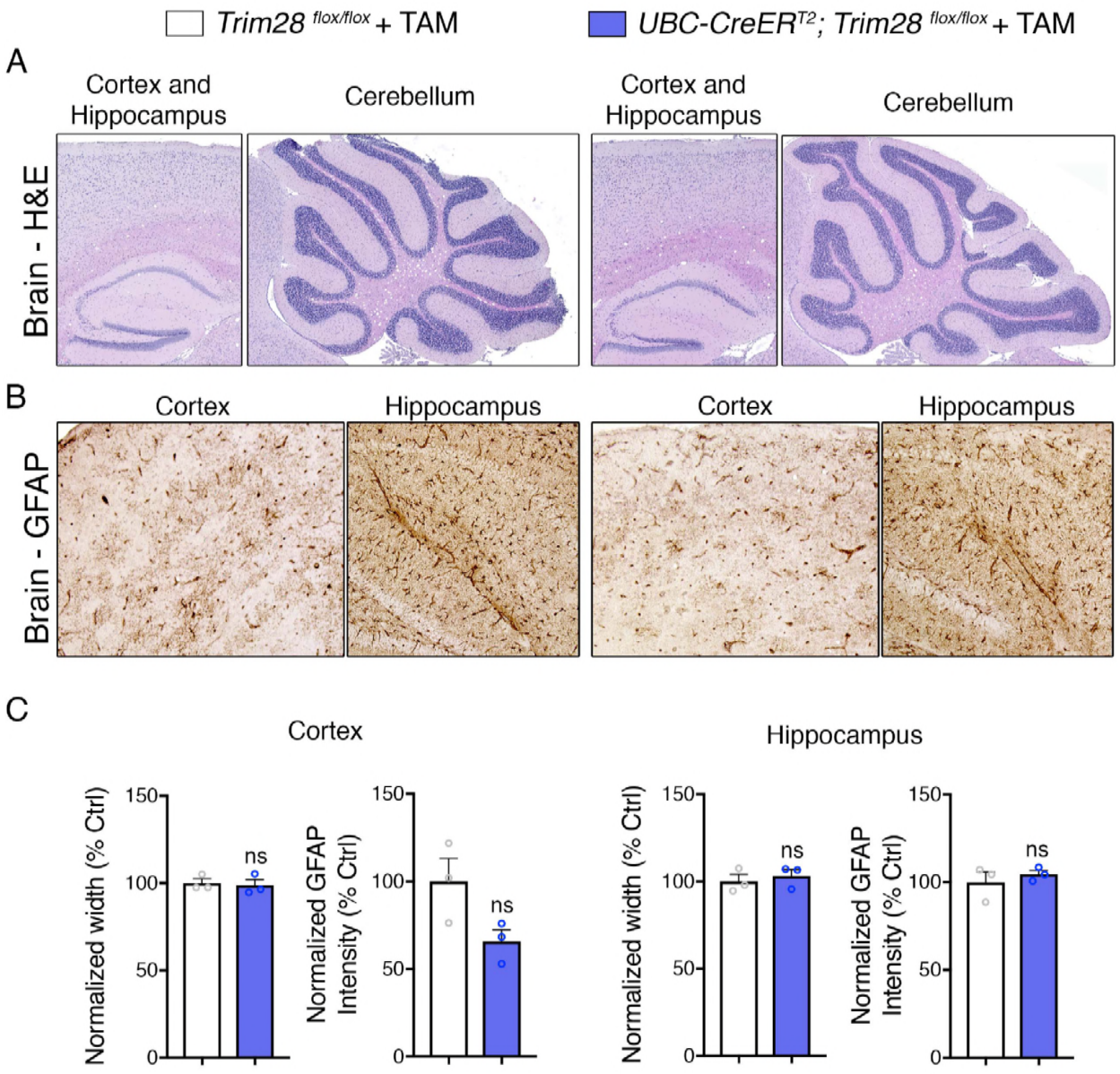

Figure 4

Figure 4. Adult depletion of Trim28 does not cause pathological abnormalities in the adult brain.

Representative photomicrographs of the cortex, hippocampus and cerebellum stained with (**A**) H&E and (**B**) GFAP. (**C**) Quantification of cortical and hippocampal width as well as normalized GFAP intensity. For each test, $n = 3$; ns denotes $P > 0.05$.

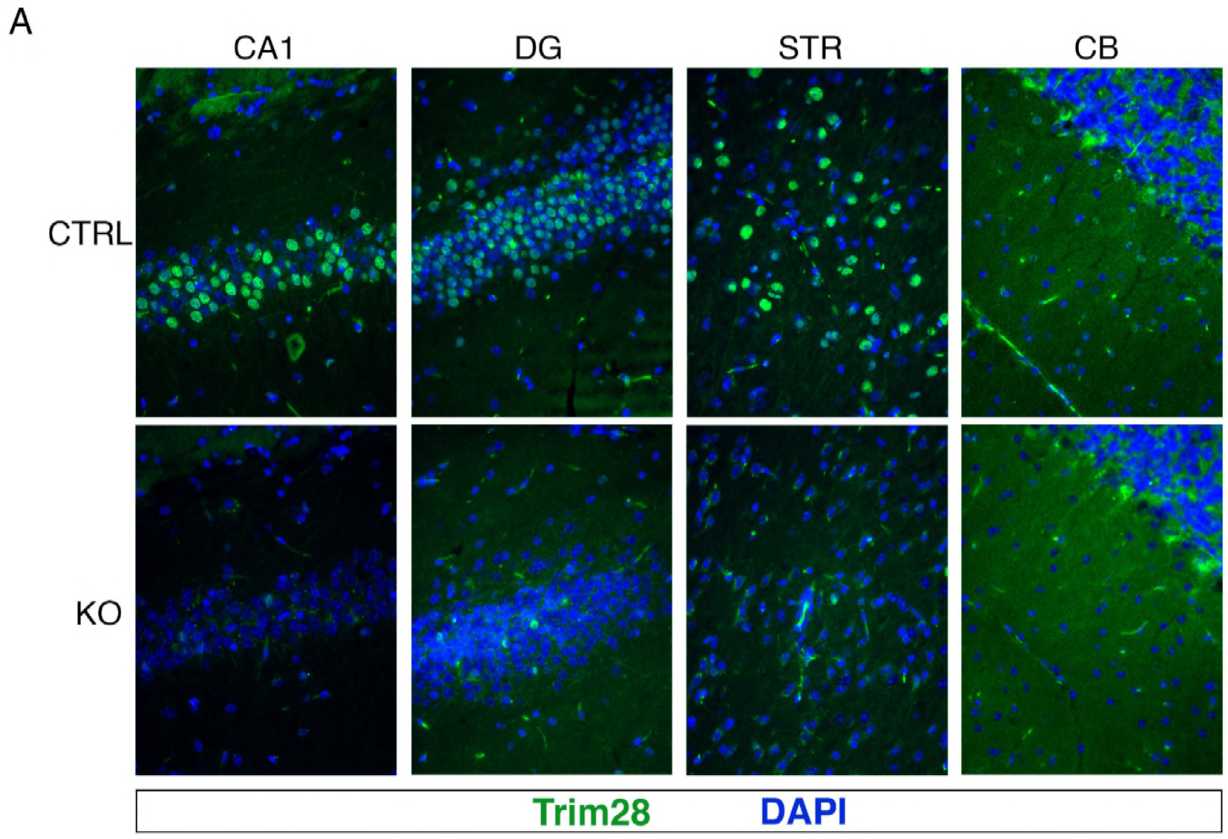

Figure 4 - figure supplement 1

Figure 4-figure supplement 1. Trim28 is expressed in the adult brain and can be effectively excised

464 from adult mice. (**A**) Representative photomicrographs of Trim28 staining in the CA1 and dentate gyrus
465 (DG) of the hippocampus, striatum (STR) and cerebellum (CB) in Trim28 adult knockouts (KO)
466 compared to littermate controls (CTRL). (**B**) qPCR on genes previously reported to be disrupted upon
467 Trim28 loss in the juvenile hippocampus.

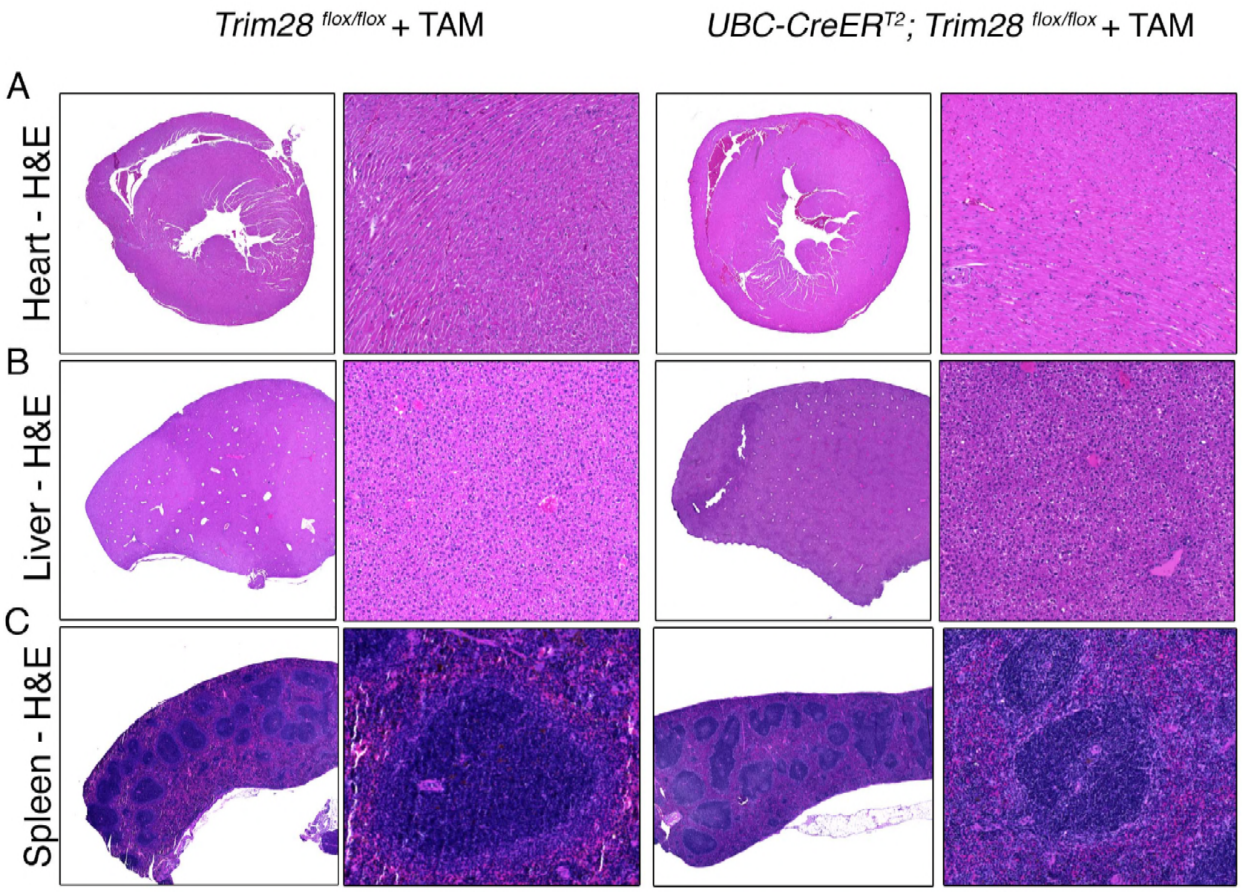

Figure 4 - figure supplement 2

Figure 4-figure supplement 2. Adult depletion of Trim28 does not cause peripheral pathological

470 abnormalities. Representative photomicrographs of (**A**) Heart, (**B**) Liver, and (**C**) Spleen from Trim28

471 adult knockouts compared to littermate controls stained for hematoxylin and eosin.

Analyte	Units	*Trim28*$^{flox/flox}$ + TAM			*UBC-CreERT2; Trim28*$^{flox/flox}$ + TAM			Adj. P-value
		Average	s.e.m.	*n*	Average	s.e.m.	*n*	
Complete blood chemistry								
CHOL	mg/dL	**37.2**	10.4	5	**83.6**	2.3	5	**0.050**
TRIG	mg/dL	**41.4**	5.5	5	**82.2**	9.0	5	0.091
ALT	U/L	**25.8**	1.6	5	**24.6**	8.0	5	1.000
AST	U/L	**59.2**	3.6	5	**124.8**	83.1	5	1.000
ALP	U/L	**93.8**	15.5	5	**55.2**	5.1	5	0.588
GLU	mg/dL	**168.6**	13.5	5	**146.6**	25.5	5	1.000
PHOS	mg/dL	**8.2**	0.5	5	**8.3**	0.4	5	1.000
Ca	mg/dL	**4.5**	1.5	5	**6.0**	1.7	5	1.000
TP	g/dL	**4.7**	0.1	5	**4.6**	0.1	5	1.000
ALB	g/dL	**2.9**	0.1	5	**2.9**	0.1	5	1.000
GLOB	g/dL	**1.7**	0.1	5	**1.8**	0.1	5	1.000
A/G	-	**1.7**	0.1	5	**1.7**	0.1	5	1.000
BUN	mg/dL	**20.6**	1.7	5	**19.6**	0.7	5	1.000
CREAT	mg/dL	**0.1**	0.0	5	**0.1**	-	5	n/a
TBIL	mg/dL	**0.2**	0.0	5	**0.2**	0.0	5	n/a
Na	mEq/L	**157.6**	2.5	5	**152.8**	2.6	5	0.985
K	mEq/L	**5.0**	0.1	5	**5.6**	0.7	5	1.000
Cl	mEq/L	**114.8**	1.7	5	**114.2**	0.7	5	1.000
Na/K	-	**31.5**	0.8	5	**29.0**	3.2	5	1.000
Iron panel								
Fe	µg/dL	**37.7**	25.3	3	**54.3**	25.5	4	1.000
TIBC	µg/dL	**245.5**	68.0	3	**349.0**	14.7	4.0	0.937
FERR	ng/mL	**487.4**	31.4	3	**463.6**	26.7	4.0	1.000
TRFN	mg/dL	**77.5**	1.6	3	**80.0**	1.5	4.0	0.997

Abbreviation	Test name
CHOL	Cholesterol, Total
TRIG	Triglycerides
ALT	Alanine Aminotransferase
AST	Aspartate Aminotransferase
ALP	Alkaline Phosphatase
GLU	Glucose
PHOS	Phosphorus
Ca	Calcium, Total
TP	Protein, Total
ALB	Albumin
GLOB	Globulin
A/G	Albumin/Globulin ratio
BUN	Urea Nitrogen
CREAT	Creatinine
TBIL	Bilirubin, Total
Na	Sodium
K	Potassium
Cl	Chloride
Na/K	Sodium/Potassium ratio
Fe	Iron
TIBC	Iron Binding Capacity, Total
FERR	Ferritin
TRFN	Transferrin

Figure 4 - figure supplement 3

Figure 4-figure supplement 3. Loss of Trim28 in adult mice does not disrupt global blood chemistry or

474 iron homeostasis. Complete blood chemistry of Trim28 adult knockout mice compared to control
475 littermates. Adjusted *P*-values from multiple t-tests (Holm-sidak corrected) for each value are presented
476 on the right. Legend for each analyte is presented below.